The comparison is again shown in Figure A2. Agreement is not so good in this case, as expected. However, we should reiterate that this is a worst case example which perhaps suffers further in accuracy from the choice of a correlation for h_{fs} which predicts $Nu_{fs} \to 0$ as $Re \to 0$. In the vast majority of cases, having substantially lower k_{rs}/k_g, higher Re, and perhaps larger d_t/d_p, the accuracy will be as good if not better than that shown in the upper diagram of Figure A2.

Manuscript received July 12, 1978; revision received March 1, and accepted March 23, 1979.

Hot Wire Measurement in the Interacting Two-Plane Parallel Jets

SHINICHI YUU
FUMIO SHIMODA
and
TOMOSADA JOTAKI

Kyushu Institute of Technology
Tobata, Kitakyushu 804, Japan

This study presents the data of turbulence properties in the two-plane parallel air jets which merge as they issue into still surroundings. These turbulent properties (time averaged and root mean square velocities, Eulerian auto and cross correlation coefficients, various scales of turbulence, energy spectra, and probability density functions of fluctuating velocities) were measured in both the converging and combined regions of the jets by using the X array, hot wire anemometers.

The negative high shear stress existed in the merging region. Strictly speaking, the turbulent flow in this region is not isotropic. In the combined region, the turbulent mechanics of these jets are essentially the same as that of the single plane jet. All of the spectra in these jets had a slope of 5/3 over about one decade of the wave number space. The probability density functions were Gaussian except for the boundary to the surrounding air.

SCOPE

Two parallel jets interact with each other and tend to merge into a single jet at the downstream of the jets when they issue from adjacent two nozzles into still surroundings. The interacting turbulent jets are able to accomplish rapid and complete mixing of fluids. These flows have numerous important applications, for example, thrust augmentors, waste disposal plumes from stacks and combustion systems, and significant problems of turbulent diffusion. The mechanism of these apparatus and systems is dominated by the turbulence phenomena of the flow in the jets.

Miller and Comings (1960) and Marsters (1977) have studied the mean flow quantities and the intensities of the turbulent velocity in interacting two plane jets. Becker and Booth (1975) have reported the data of the mean smoke concentration and the intensities of the turbulent concentration in two round jets with nozzle axes intersecting. However, no information about other important turbulent properties in the interacting jet flow is available in the literature.

The main difficulty confronted in application of turbulent theories to various engineering operations comes from insufficient information about the turbulent structure. Hence, in this study, detailed various turbulence properties (time averaged and root mean square velocities, Eulerian auto and cross correlation coefficients, various scales of turbulence, energy spectra, and probability density functions of fluctuating verocities) wire measured in the interacting two plane parallel jets.

Turbulence properties were measured in order to supply engineering information and to give experimental data on which a realistic model of the turbulent flow can be based.

The objective of this work is to describe the flow of air in interacting plane jets with particular emphasis on the structure of turbulence in order to contribute basic data to various engineering operations.

CONCLUSIONS AND SIGNIFICANCE

A very complete picture of the flow pattern in the interacting two-plane parallel jets has been obtained. Time averaged velocity profiles showed that they are not similar in the converging region but that they exhibit a high degree of similarity and are the same as that of a single-plane jet in the combined region. Similarity means that there are one velocity scale and one length scale which are sufficient to make the distributions of reduced velocities in terms of reduced coordinates identical. The results also indicated that the distance from the nozzle exit to the merge point of the ventilated jets is about six times as long as that of unventilated jets. This showed that ventilated jets interact more weakly than unventilated jets because of the air ventilation between jets.

The three components of root mean square turbulent velocity in the interacting two parallel jets have been measured for the first time. These measurements indicated that the value of the longitudinal component $\sqrt{\overline{u'^2}}$ is about 1.2 to 1.5 times that of the lateral component $\sqrt{\overline{v'^2}}$, and $\sqrt{\overline{v'^2}}$ is nearly equal to the transverse component $\sqrt{\overline{w'^2}}$. Hence, strictly speaking, the turbulent flow field is not totally isotropic. Comparing these results of two jets with that of a single jet, there are significant differences in both shape and height between them in the converging region.

The cross correlation coefficients are fairly large except for the jet center line. The cross correlogram is negative in the region between the two jets. This describes the interaction and the merging of the two jets.

The integral length scales (Λ_x, Λ_y, and Λ_z) were nearly constant across the jet flow, and all of them grow linearly with the longitudinal distance. Similar conclusion have been drawn from the results of the dissipation length scales (λ_x, λ_y, and λ_z). The isotropic relations of small scale motion that $\Lambda_x = 2\Lambda_y$, $\Lambda_y = \Lambda_z$, $\lambda_x = \sqrt{2}\lambda_y$, and $\lambda_y = \lambda_z$ were well supported. This means that the small scale motion of the two jets is isotropic. The averaged dissipation scale was about 1/5 times the averaged integral length scale.

The normalized one-dimensional energy spectra were nearly the same everywhere in the interacting two jets. The spectra had a slope of $-5/3$ over about one decade of the wave number space. Further, $E_2(k_1)$, whose integral is $\overline{v'^2}$, was nearly equal to $E_3(k_1)$, whose integral is $\overline{w'^2}$, and $E_2(k_1)$ and $E_3(k_1)$ are larger than $E_1(k_1)$, whose integral is $\overline{u'^2}$, in this subrange. This agreed with the locally isotropic inertial subrange relation $E_2(k_1) = E_3(k_1) = 4/3\, E_1(k_1)$.

The probability density functions of the fluctuating velocity for the most part of the interacting two jets were Gaussian shape, which is typical of homogeneous turbulence. Hence, the flow field in the interacting two plane jets is nearly homogeneous and locally isotropic.

The body of the data presented in this study are useful to various engineering operations and to present a realistic model of the turbulent flow.

PREVIOUS WORK

Rummel (1937) first measured the mean concentration field of interacting two round jets with nozzle axes intersecting at various angles to each other with the flow converging. Corrsin (1944) measured mean flow directions, mean temperature distributions, and total heads in the unstable flow from free standing seven parallel slits. Baron and Bollinger (1952) measured the mean velocity distribution of interacting round jets to examine the validity of the superposition principle of the momentum flux based on Reichardt hypothesis. Their results show that the principle is accurate only at small intersecting angles. Makaroff and Khudenko (1965) and Kirillov and Khudenko (1965) studied the direction taken by the jet resulting from the interaction of two others. Miller and Comings (1960) experimentally studied the flow field in the interacting two-plane parallel jets issuing from a solid wall into still air. We also call such type of jets unventilated as the interacting two-plane parallel jets issuing from a solid wall into still air according (Marsters, 1977). Miller and Comings indicated that remarkable negative pressure is observed in the confined region between the jets and that it causes the jet flows to be deflected inwards so that the jets merge with each other and two large counterrotating vortices in the confined region. They also showed that the mean flow of the combined jet exhibits the same characteristics of a single jet flow. Knystautas (1964) measured the mean velocity profiles in the unventilated jet flow from a series of closely spaced uniform holes in line and examined the possibility of obtaining two-dimensional turbulent jet flow from these holes. His results indicated that fully merged two-dimensional flow occurs at approximately twelve hole spacings downstream of the exit plane.

Tanaka (1970, 1974) measured the intensity distributions of longitudinal fluctuating velocities in the two-plane unventilated jets' by using a single, hot wire anemometer. His data indicated that the turbulent intensity at the center line of the combined jet is larger than that of a single jet. Recently, Marsters (1977) has experimentally examined the mean flow quantities in two-plane parallel jets issuing from free standing nozzles such that secondary flow can be entrained between them and compared with predictions based on an integral model of the flow. We call such types of jets ventilated as two-plane parallel jets issuing from free standing nozzles such that secondary flow can be entrained between them (Marsters, 1977). Marsters' results indicate that the mean velocity distributions exhibit self-preserving behavior in both the upstream and the downstream of the merge point except for the merging region. Becker and Booth (1975) present the data of the mean smoke concentration field and the intensity of the turbulent concentration fluctuation in two

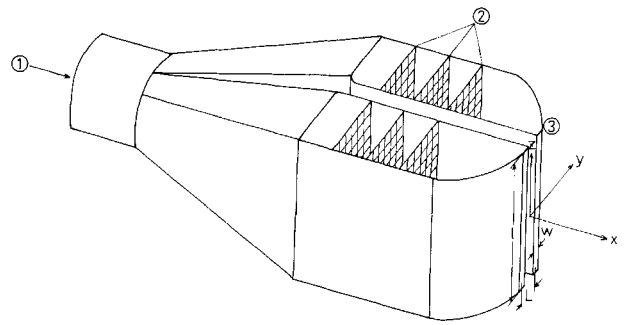

Fig. 1. Experimental setup.

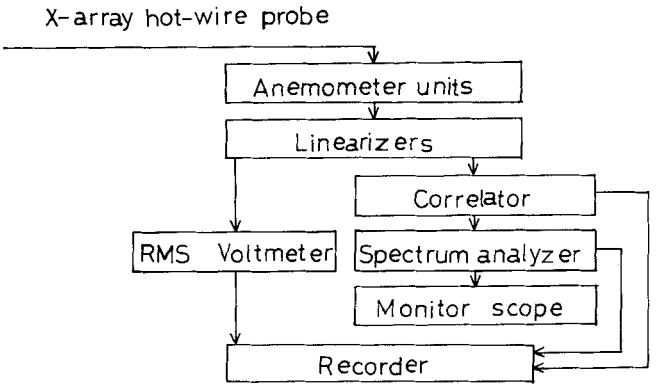

Fig. 2. Schematic diagram of measurement system.

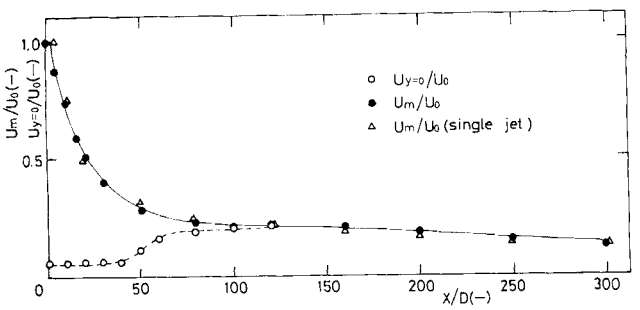

Fig. 3. Maximum time averaged velocity decay.

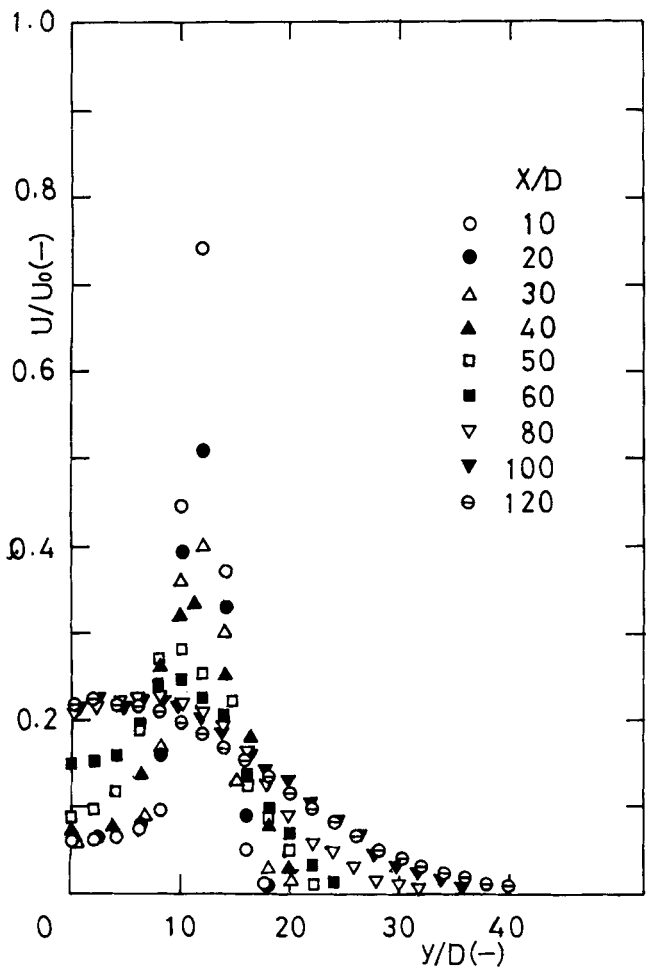

Fig. 4. Time averaged longitudinal velocity profiles upstream of merge point.

round jets with nozzle axes intersecting at half angles of 15, 30, and 45 deg. They used the smoke scattered light technique. They also derived the relation between the intensity and the covariance of the turbulent concentration fluctuations.

As mentioned above, there is relatively little information of turbulent properties available on interacting two jets, especially plane ventilated jets. Hence, we measured various turbulent characteristics of the flow in the interacting two-plane parallel ventilated jets by using X array, hot wire anemometers. X array, hot wire technique was used because it makes it possible to measure the components of fluctuating velocity, and its frequency response is extremely good.

EXPERIMENTAL APPARATUS AND PROCEDURE

The experimental setup is shown in Figure 1. Compressed air was used, which led to a storage tank from which it entered the plenum chamber ①. From the plenum chamber, air passed through three 18 mesh brass gride ② and converged to nozzle exits ③. The grids were located for producing a uniform velocity along the length of the slit. The jets issued from slit nozzles of width $D = 2.0$ mm and length $l = 150$ mm. The contraction ratio was 15. In this case, the velocity profiles are flat both across and along the jet. The 75:1 aspect ratio was considered to be adequate for two dimensionality of flow for each jet. Trentacoste and Sforza (1967) showed that for aspect ratio of 40, the center-line velocity decay and the velocity profiles are typical of those for plane jet up to about 200 jet widths downstream. Air flow rates to the two nozzles were equal and constant within ±3% variation. The distance L between the center lines of the two nozzles were set equal to twenty-four times nozzle widths. The resulting two-plane parallel jets exhausted into the large chamber confined between two vertical walls extending 1.5 m downstream from the nozzle exit and 0.4 m to either side of the center line. The X array, hot wire probe was installed on the traversing equipment. The turbulence properties were measured at fourteen distances from the nozzle exit, that is, $x/D = 10$ to 300. Data were taken at about twenty different points in each cross section. The issuing velocity was kept at 47 m/s for these tests. The Reynolds number of the mean flow based on the nozzle width was 6 300. The coordinate system used in this study is also seen Figure 1.

The turbulence and mean velocity measurements were made by using KANOMAX constant temperature, hot wire anemometers with type 29-1141 X array, hot wire probes. The probe was a platinum coated tungsten wire, 5 μm diameter, 1 mm long, and a cold resistance of 4 to 7 ohms. A low pass filter of 20 KHz built into the anemometer circuit was used to discard the electric noise. The wires were calibrated before and after every run in a 5 × 5 cm exhaust plane of a nozzle, where the turbulence level was about 0.5%. To estimate the effects of differences between ambient and calibration temperatures on hot wire output, the temperature was measured continuously

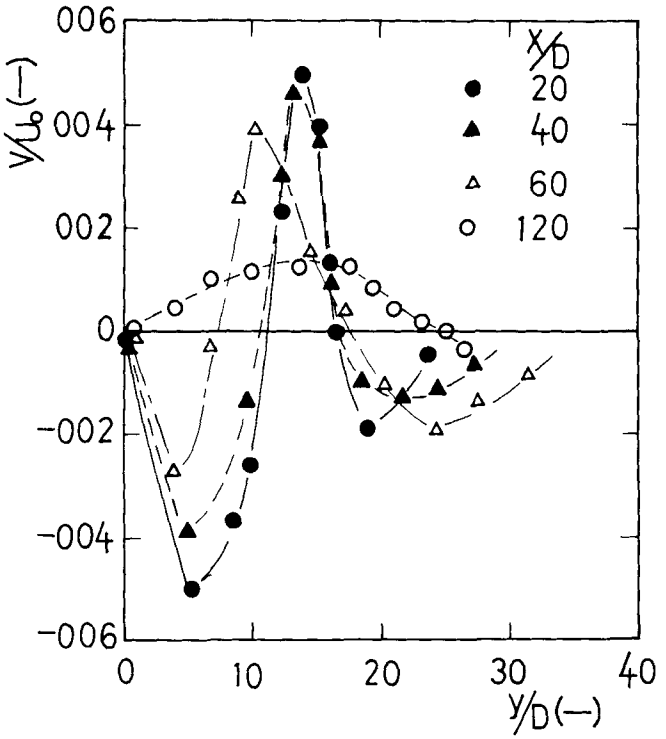

Fig. 5. Time averaged lateral velocity profiles upstream of merge point.

with a thermometer. All results in this report have been corrected for ambient temperature changes where applicable.

The frequency response of the anemometers was found to be such that the 3db down point was over about 25 KHz which is much higher than the highest frequency of interest. A schematic drawing of measurement system used for the analysis is shown in Figure 2. The auto and cross correlation functions were obtained by using a TEAC type C-120 real time digital correlator. The correlation function was observed on an oscilloscope and also recorded on an X-Y recorder. The upper frequency limit of correlator (1 MHz) was well above the highest frequency of interest in this study at all time delay ranges. The sampling time of correlator ranged from 0.5 μm to 50 s. The amplitude spectra were obtained with a TEAC type F-120 spectrum analyzer. The frequency range covered was from 0.01 Hz to 1 MHz. The frequency resolution power ranged from 10.6 KHz to 0.000106 Hz. The amplitude probability density functions were computed by using a TEAC type C-120 probability density computer. The amplitude spectra and probability density functions were also recorded on a X-Y recorder.

RESULTS AND DISCUSSION

At the nozzle exit, the z direction traverse was carried out to determine the degree of uniformity of the flow from these nozzles. Traversing showed a flat profile with a slight rounding near the end. The time averaged velocity was 97% of the maximum value over the middle 80% of the span of the nozzle. All data in this report were taken in the $z = 0$ plane. Measurements revealed a high degree of flow symmetry about the center line. Hence, one side of the data is reported.

Time Averaged Velocity Profile

Figure 3 shows the maximum time averaged velocity decay (jet center-line velocity decay) and the time averaged velocity distribution on the x axis in the interacting two-plane parellel ventilated jets. If we compare the jet center-line velocity decay of the interacting plane ventilated jets with that of a plane single jet, these plots indicate that the interacting plane jets decay as if they were

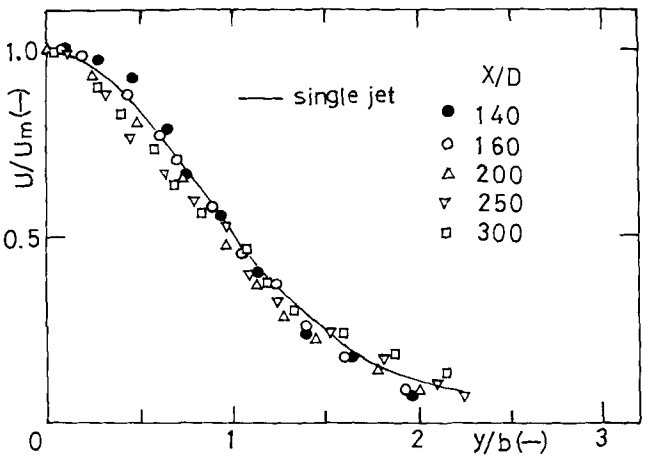

Fig. 6. Time averaged longitudinal velocity profiles downstream of merge point.

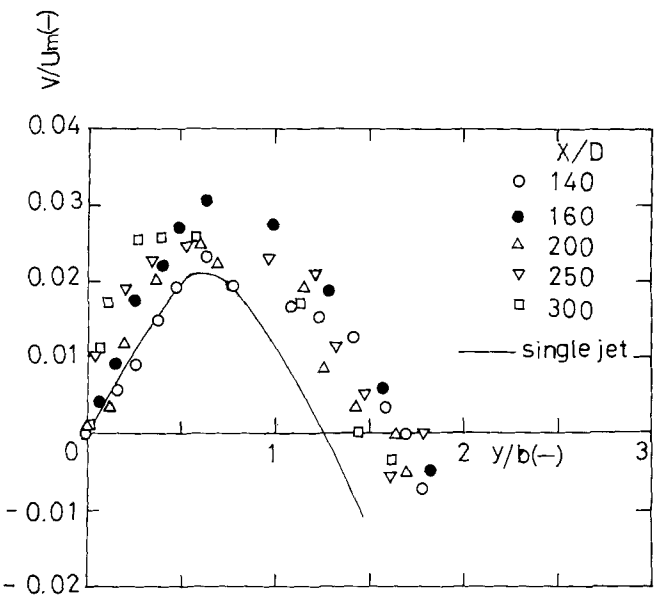

Fig. 7. Time averaged lateral velocity profiles downstream of merge point.

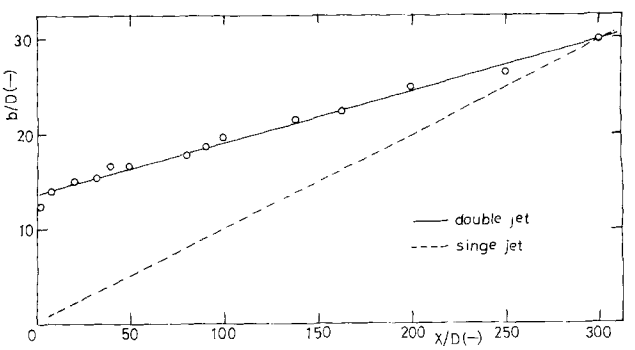

Fig. 8. Jet half width.

a two-dimensional single jet flow. At $x/D = 120$, the trajectory of the jet center line of the interacting jet coincides with that of the velocity on the x axis. Hence, it seems that the initially individual jets have merged at this point, and the flow variables resembled those of a single jet flow.

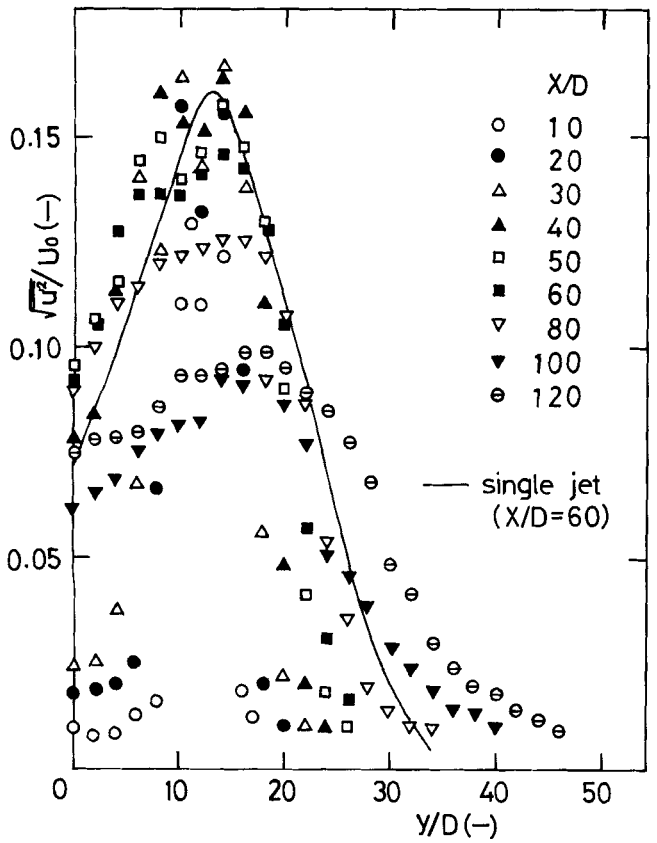

Fig. 9 (a). Distributions of the longitudinal fluctuating velocity upstream of merge point (x/D = 10 to 40). (b) Distributions of the longitudinal fluctuating velocity upstream of merge point (x/D = 50 to 120).

The time averaged longitudinal and lateral velocity profiles for points upstream of merge point are shown in Figures 4 and 5, respectively. These figures indicate the process whereby two jets interact and merge with each other. These plots in Figures 4 and 5 confirm that the interacting two ventilated jets merge at the point $x/D \fallingdotseq 120$. This is in good agreement with the result of Marsters (1977) for interacting two-plane ventilated jets. Here we define this point $x/D = 120$ as the merge point. If we compare the value of this merge point of ventilated jets with that of unventilated jets measured by Tanaka (1970) under the same condition, the former is about six times the latter. It shows that ventilated jets interact more weakly than unventilated jets because of the air ventilation between jets. As shown in Figures 4 and 5, the velocity profiles are not similar in the upstream of the merge point.

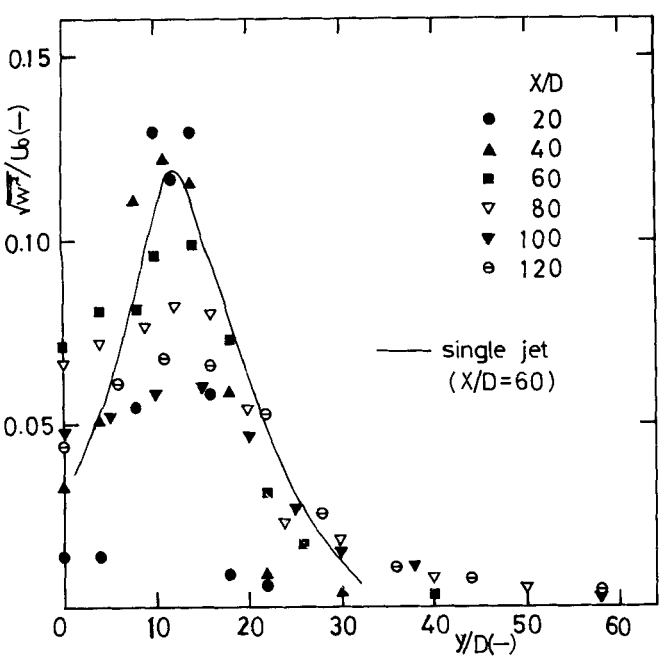

Fig. 11. Distributions of the transverse fluctuating velocity upstream of merge point.

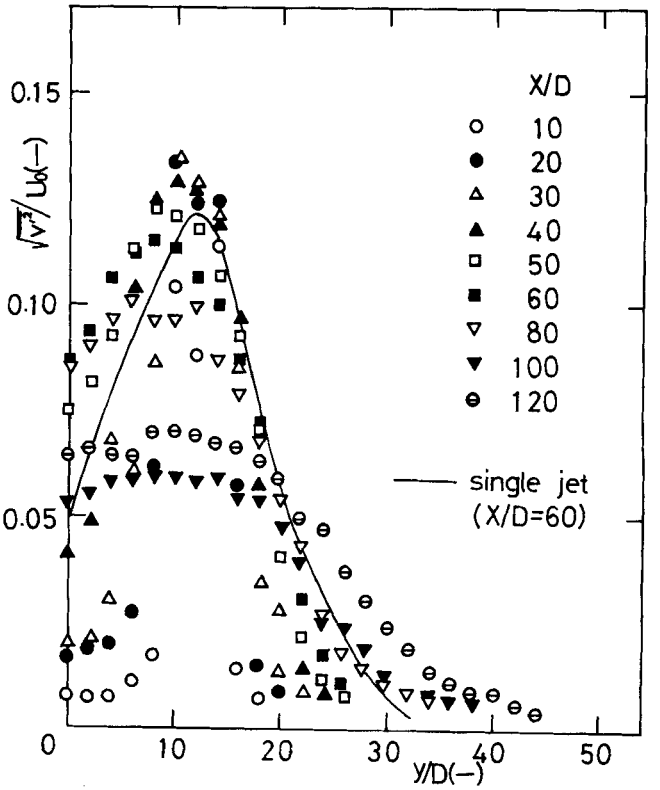

Fig. 10 (a). Distributions of the lateral fluctuating velocity upstream of merge point (x/D = 10 to 40). (b) Distributions of the lateral fluctuating velocity upstream of merge point (x/D = 50 to 120).

The downstream longitudinal and lateral velocity profiles are shown in Figures 6 and 7, respectively. The longitudinal jet velocity profile plotted against y/b exhibits a high degree of similarity and is the same as that of a plane single jet. The lateral profiles are nearly similar and fairly larger than that of a plane single jet.

The dimensionless jet half width b/D vs. downstream distance x/D is plotted and compared with that of a single plane jet in Figure 8. As expected, the curve is linear except the region near the nozzle exit. The gradient of b/D curve is smaller than that of a single-plane jet, since two parallel jet flows are deflected inwards.

Turbulent Intensity

The profiles of three components of root mean square turbulent velocity for points upstream of merge point (converging region) are shown in Figures 9, 10, and 11, respectively. The examination of the plots in these figures reveals that near the nozzle exit the two peaks occur on the points which correspond to both lips of the nozzle. Near $x/D \fallingdotseq 10$, both peaks (inner peak and outer peak) of $\sqrt{\overline{u'^2}}$ and $\sqrt{\overline{v'^2}}$ begin a period of rapid growth. Downstream from $x/D \fallingdotseq 30$, the inner peak of $\sqrt{\overline{u'^2}}$ spreads

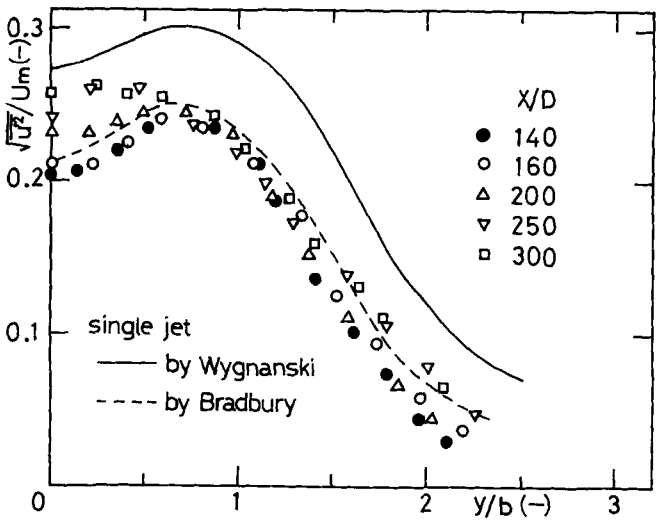

Fig. 12. Distributions of the longitudinal fluctuating velocity downstream of merge point.

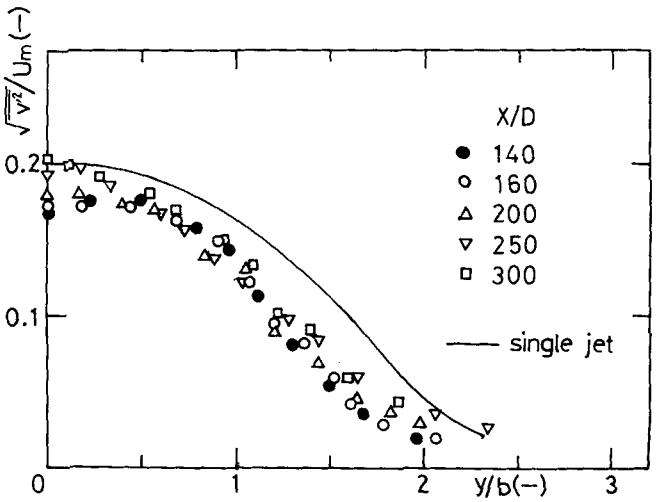

Fig. 13. Distributions of the lateral fluctuating velocity downstream of merge point.

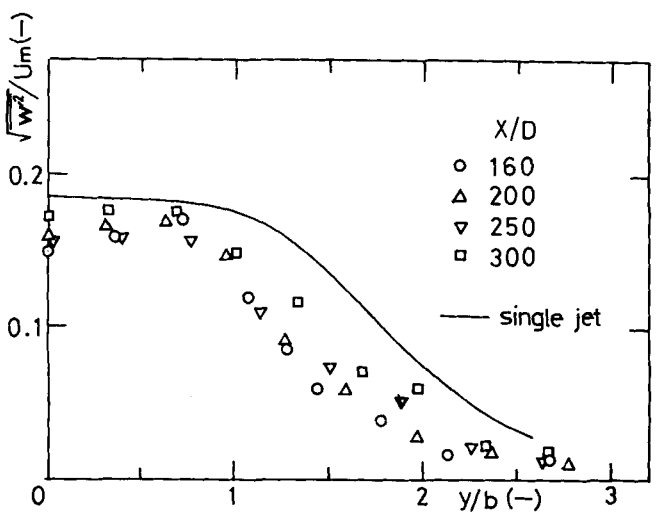

Fig. 14. Distributions of the transverse fluctuating velocity downstream of merge point.

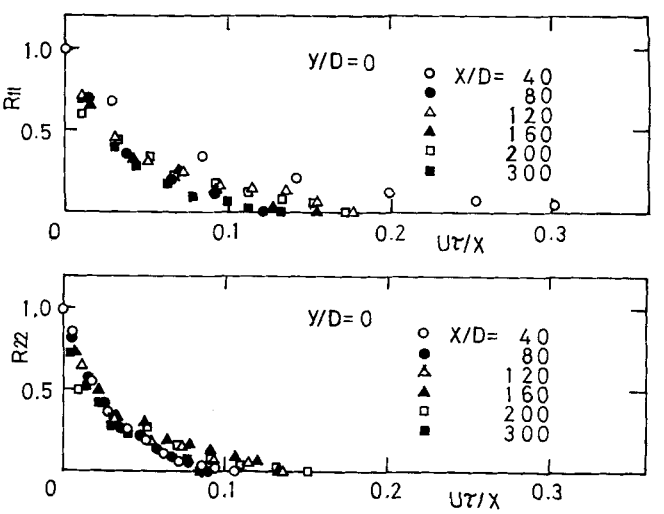

Fig. 15. Eulerian autocorrelation coefficient.

more rapidly than the outer peak and develops a hump clearly evident at $x/D = 60$. On the contrary, the inner peak of $\sqrt{\overline{v'^2}}$ spreads more slowly than the outer peak. Downstream from $x/D \doteqdot 40$, in the region where the two jets intermingle, the inner peak of $\sqrt{\overline{u'^2}}$ decays quite rapidly, and at $x/D = 80$ a trace of an inner peak of $\sqrt{\overline{u'^2}}$ does not remain. Downstream from $x/D \doteqdot 20$, the outer peaks of $\sqrt{\overline{v'^2}}$ and $\sqrt{\overline{w'^2}}$ decay rapidly, and at $x/D \doteqdot 40$ no trace of outer peaks of $\sqrt{\overline{v'^2}}$ and $\sqrt{\overline{w'^2}}$ remains. The solid lines in Figures 9*b*, 10*b*, and 11 indicate Gutmark and Wygnanski's (1976) data of a single-plane jets. As compared with our results of two jets, it is noted that there are significant differences in both shape and height between them. The reason is that the strong interaction of individual flow fields exists in the upstream of merge point of two-plane jets.

The comparison of three turbulent components with each other revealed that the value of $\sqrt{\overline{u'^2}}$ is about 1.2 times as large as that of $\sqrt{\overline{v'^2}}$, and that $\sqrt{\overline{v'^2}}$ is nearly equal to $\sqrt{\overline{w'^2}}$.

The profiles of three components of root mean square turbulent velocity for downstream of merge point (combined region) are shown in Figures 12, 13, and 14. U_m and b were used in normalizing the ordinate and the abscissa in these figures in order to indicate the existence of similarity in the combined region of the jets.

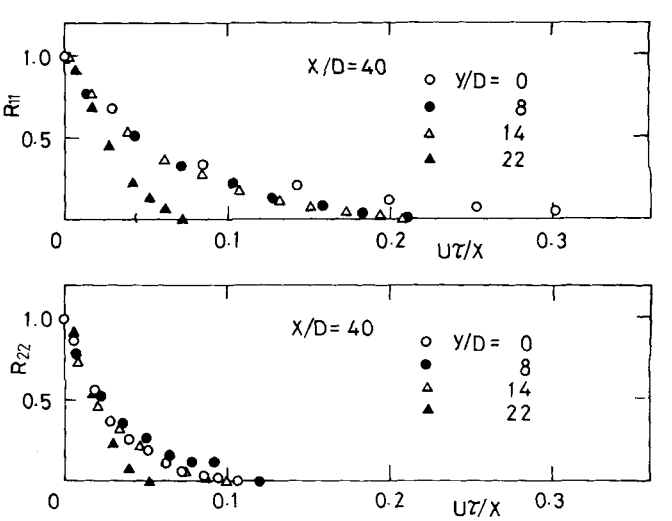

Fig. 16. Lateral traverses of R_{11} and R_{22} in the converging region.

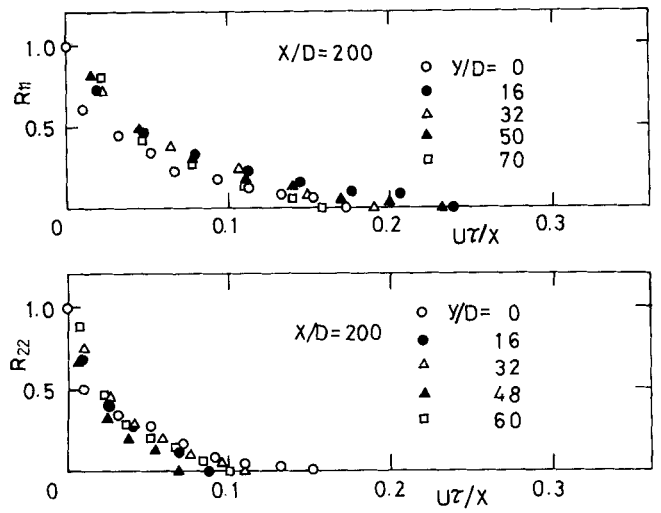

Fig. 17. Lateral traverses of R_{11} and R_{22} in the combined region.

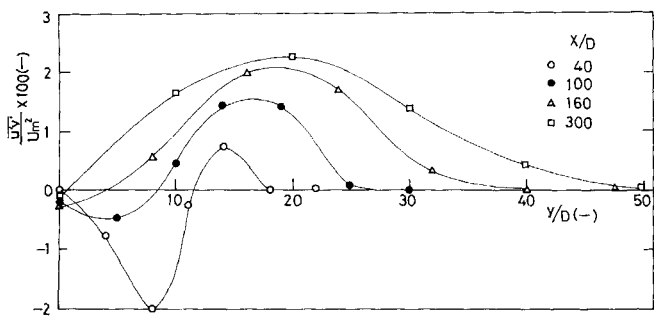

Fig. 19. Distributions of the turbulent shear stress.

Profiles plotted against y/b, that is, Figures 12, 13, and 14, exhibits similarity. The same cannot be said for the profiles shown in Figures 9, 10, and 11. The solid lines in these figures indicate Gutmark and Wygnanski's (1976) data of a single plane jet. As should be expected, the downstream development of the turbulent intensity resembles that of a single jet flow. As shown in these figures, all of the profies are typical in shape to those obtained in a single jet flow. Gutmark and Wygnanski's data of a single-plane jet are somewhat larger than those of the interacting two-plane jets; however, Bradbury's (1965) data of a single-plane jet in Figure 12 are in good agreement with those of the interacting two-plane jets. The value of $\sqrt{\overline{u'^2}}$ for the downstream is about 1.5 times that

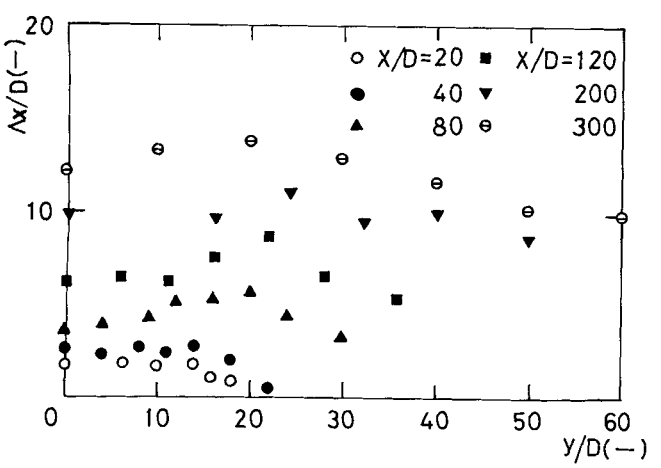

Fig. 20. Distributions of the longitudinal integral length scales.

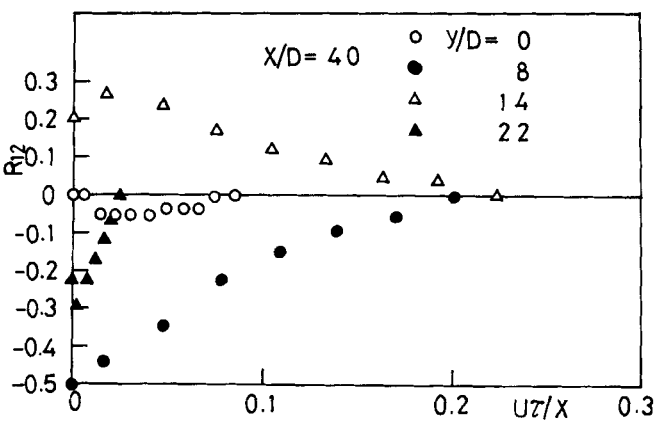

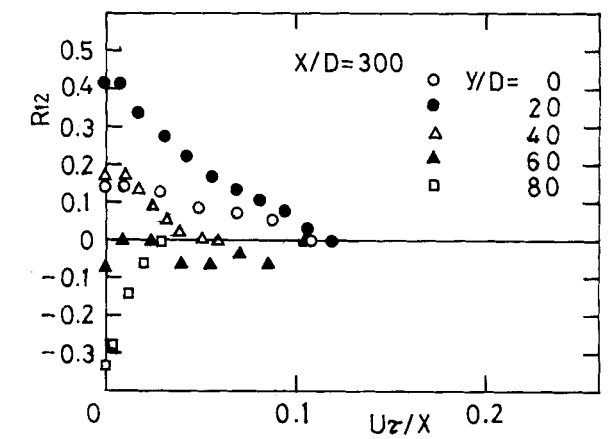

Fig. 18. Lateral traverses of Eulerian cross-correlation coefficient R_{12}.

of $\sqrt{\overline{v'^2}}$, and $\sqrt{\overline{v'^2}}$ is also nearly equal to $\sqrt{\overline{w'^2}}$. Hence, strictly speaking, the turbulent flow field is not totally isotropic.

Eulerian Correlations

Generally, the Eulerian correlation coefficient is defined as

$$R_{ij}(\tau) = \frac{\overline{u_i'(t)u_j'(t+\tau)}}{\sqrt{\overline{u_i'^2(t)}}\sqrt{\overline{u_j'^2(t+\tau)}}} \qquad (1)$$

$R_{ij_{i=j}}(\tau)$ and $R_{ij_{i=j}}(\tau)$ are auto and cross correlation coefficients, respectively. The longitudinal and lateral auto correlation coefficients are defined as, respectively

$$R_{jj}(\tau) = \frac{\overline{u'(t)u'(t+\tau)}}{\sqrt{\overline{u'^2(t)}}\sqrt{\overline{u'^2(t+\tau)}}} = R_{x,x}(\tau) \qquad (2)$$

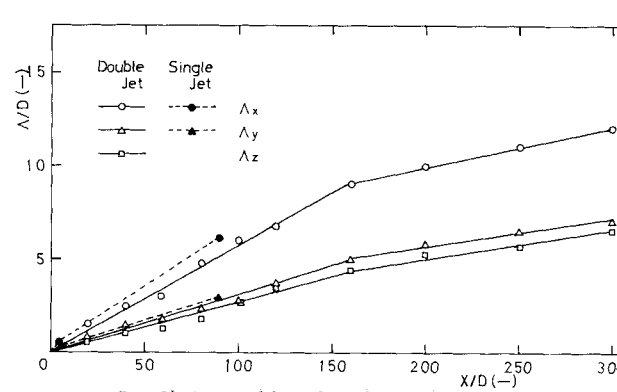

Fig. 21. Integral length scales on the x axis.

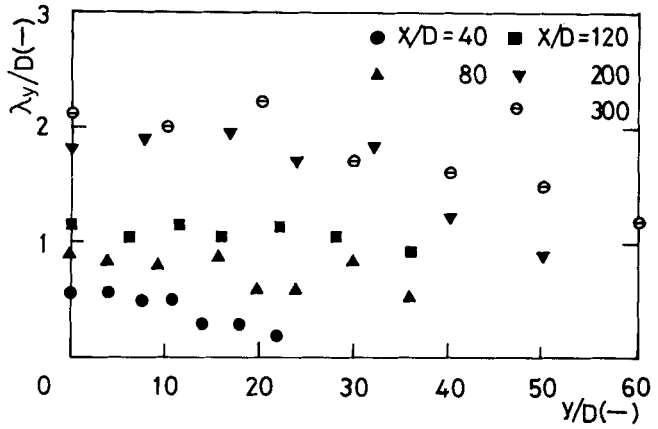

Fig. 22. Distributions of the lateral dissipation length scales.

$$R_{22}(\tau) = \frac{\overline{v'(t)v'(t+\tau)}}{\sqrt{\overline{v'^2(t)}}\sqrt{\overline{v'^2(t+\tau)}}} = R_{yy}(\tau) \qquad (3)$$

In Figure 15, the representative autocorrelation coefficients at $y/D = 0$ and various x/D are plotted vs. $U\tau/x$. The results, falling nearly on a single curve, indicate the similarity as far as the various scales are concerned. The representative lateral traverses of coefficients in the converging region are shown in Figure 16. The curves of the correlation coefficients are equal to each other when y/D is smaller than 14 at $x/D = 40$. This value of y/D corresponds to about the half width of the jets. Outside of the jet flow, namely, $y/D > 14$ at $x/D = 40$, the correlation coefficients seem to decrease with increasing y/D. The similar traverses in the combined region are plotted

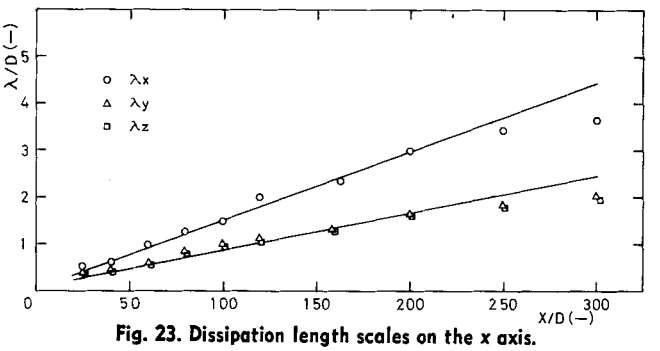

Fig. 23. Dissipation length scales on the x axis.

in Figure 17. These plots, which may be nearly expressed by one curve, show that the coefficients are constant over the cross section of the jets. In the both regions, R_{11} was two times R_{22}, and R_{22} was nearly equal to R_{33}. This suggests that $\Lambda_x = 2\Lambda_y$ and $\Lambda_y = \Lambda_z$. This is an isotropic relation of small scale motion. Hence, the small scale motion of the flow field of the two jets is isotropic.

The representative lateral tranverses of cross correlation coefficients in the converging and combined regions are shown in Figure 18. The cross correlograms are fairly large in the both regions. Hence, strictly speaking, the turbulent flow field of the two jets is not isotropic. The results in the converging region indicate that the value of the cross correlogram is negative in the region between the two jets and positive outside of the jet center line. This describes the interaction and the merging of the two jets. Farther away from the jet center line, the correlogram becomes negative again. The cross correlogram in the combined region is positive except farther from the jet center line. Reynolds stresses $\overline{u'v'}$ normalized by U_m^2 are plotted in Figure 19. The similar conclusions mentioned

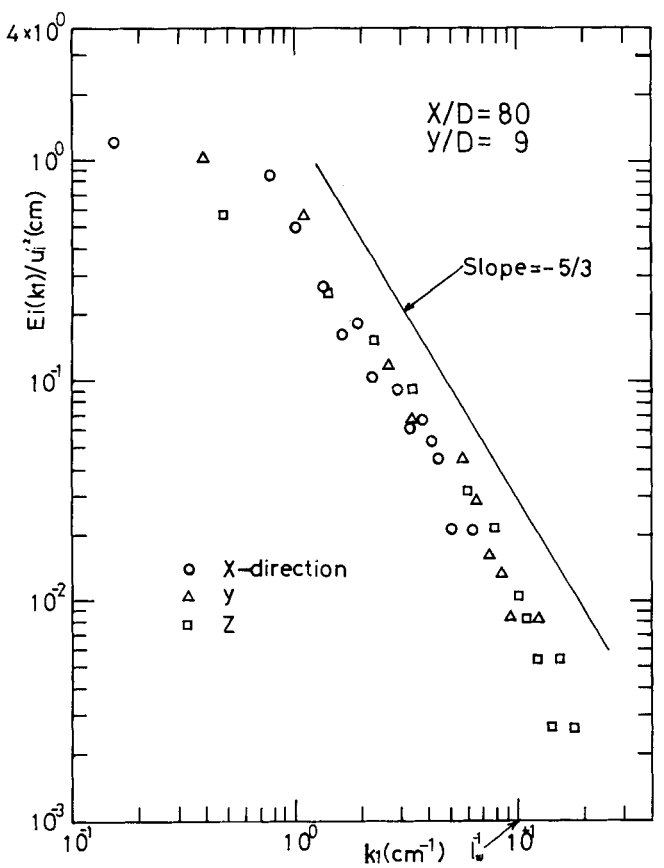

Fig. 24a. One-dimensional energy spectrum in the converging region.

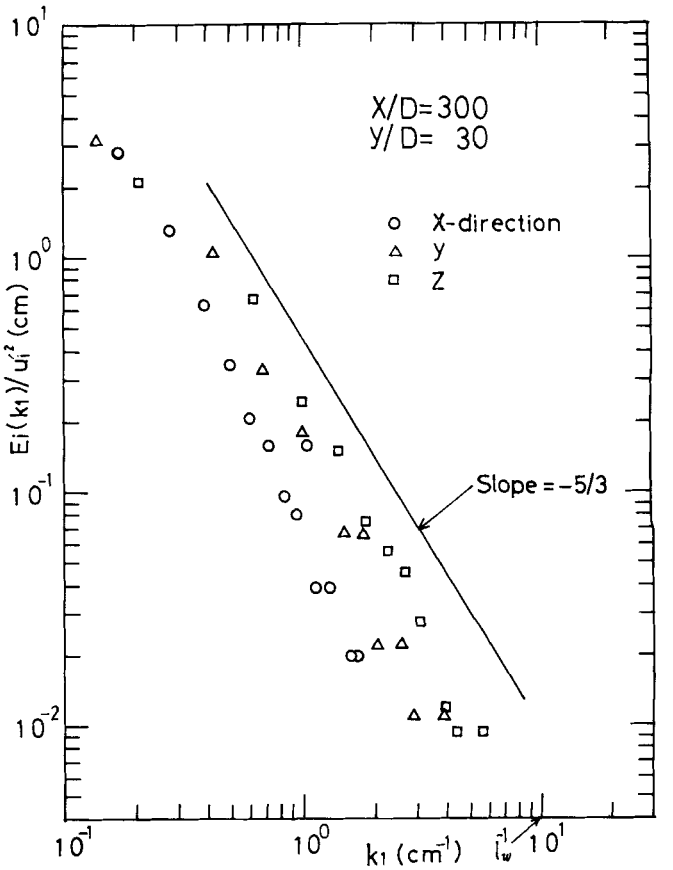

Fig. 24b. One-dimensional energy spectrum in the combined region.

above may be drawn from it. In the combined region, the normalized Reynolds stresses appear to attain their similarity distribution at a longitudinal distance as well as those of a single jet.

Scales of Turbulence

There are two types of scales that represent the important characteristics of the structure of turbulence. One of them is the Eulerian integral time scale T_{E_i} or length scale Λ_i. This scale may be considered a measure of the longest connection or correlation distance between the turbulent velocities. Another one is the Eulerian dissipation scale λ_i or time scale τ_i. This scale is a measure of the average dimension of the eddies which are mainly responsible for dissipation. The Eulerian integral time scale is obtained by integrating graphically the Eulerian auto correlation function:

$$T_{E_i} = \int_0^\infty R_{ii}(\tau)\,d\tau \tag{4}$$

The Eurelian dissipation time scale is obtained by

$$\frac{1}{\tau_i^2} = \frac{2\pi^2}{u_i'^2}\int_0^\infty n^2 E_i(n)\,dn \tag{5}$$

Each length scale for these time scales is calculated by using Taylor's hypothesis:

$$\Lambda_i = U\,T_{E_i} \tag{6}$$

$$\lambda_i = U\,\tau_{E_i} \tag{7}$$

A frozen pattern of turbulence exists when the turbulence level is low, viscous forces are negligible, and the mean shear is small. The use of Taylor's hypothesis is not strictly valid for the turbulent flow in the interacting two jets, but this is not considered a serious defect, since $U >> u$ or v.

The lateral traverses of Λ_x for various longitudinal distances are shown in Figure 20. The results indicate that Λ_x is nearly constant across the jet flow. However, closer examination reveals that at first Λ_x increases slightly with increasing outward distance, and farther away from the jet center line Λ_x decreases gradually with increasing y/D. The results also indicate an increase of Λ_x with increase of x. Similar results for Λ_y and Λ_z were obtained. The plots of the lateral traverses of Λ_y and Λ_z are omitted for the sake of simplicity.

The longitudinal traverses of Λ_x, Λ_y, and Λ_z along the y axis are plotted in Figure 21. The results show that all of the three integral length scales (Λ_x, Λ_y, and Λ_z) grow linearly with x. The rate of increase $d\Lambda_i/dx$ changes at the point $x/D \simeq 160$. $d\Lambda_i/dx$ becomes smaller in the region where $x/D > 160$. It seems that the large eddies of the interacting two jets are not preserved longer by the strong mixing. The integral scales obtained from this figure are

$$\bar{x} = x/D \leqq 160$$

$$\Lambda_z/D = 0.056\bar{x},\quad \Lambda_y/D = 0.030\bar{x},\quad \Lambda_z/D = 0.028\bar{x} \tag{8}$$

$$\bar{x} > 160$$

$$\Lambda_z/D = 0.021\bar{x} + 5.6,\quad \Lambda_y/D = 0.014\bar{x} + 2.7,$$

$$\Lambda_z/D = 0.015\bar{x} + 2.0 \tag{9}$$

Comparing these integral length scales with those of a single-plane jet by Gutmark and Wygnanski (1976), we find that they are nearly equal to each other in the region where $x/D < 128$. As there are no data of a single-plane jet in the region $x/D > 128$, the exact comparison is not possible. The results in Figure 21 indicate the isotropic relation of small scale motion that $\Lambda_x = 2\Lambda_y$ and $\Lambda_y = \Lambda_z$.

The lateral traverses of λ_y for various longitudinal distances are shown in Figure 22. The longitudinal traverses of λ_x, λ_y, and λ_z along the y axis are plotted in Figure 23. Similar conclusions mentioned above may be drawn from Figures 22 and 23. The results in these figures also show the isotropic relation of small scale motion, that is, $\lambda_x = \sqrt{2}\lambda_y$ and $\lambda_y = \lambda_z$. Therefore, the small scale motion of the two jets is isotropic. The averaged dissipation scale is about one-fifth times the averaged integral length scale. A Reynolds number based on λ_y and $\sqrt{\overline{v'^2}}$ yields values in the range 200 to 1 200. In this case, 1.5 decade of Kolmogoroff range in the energy spectrum would be expected.

One-Dimensional Energy Spectra

The fluctuating velocities can be analyzed into their harmonic components by Fourier analysis. The energy contributions of various frequencies can be obtained and presented in the form of a frequency spectrum. The spectrum in the frequency domain can be converted into wave number space. Frequency n and wave number k_1 are related as follows:

$$k_1 = 2\pi n/U \tag{10}$$

Here Taylor's hypothesis is used.

The significant information presented by the spectra is the existence of a $-5/3$ slope region (Kolmogoroff inertial subrange). In the inertial subrange, the condition that the wave number must fall in such a subrange is

$$k_e << k << k_d \tag{11}$$

k_d is obtained from

$$k_d = \frac{1}{\eta} \tag{12}$$

where $\eta = (\nu^3/\epsilon)^{1/4} \cdot k_e$ is the wave number at the maximum point in the spectrum. Another condition which should be satisfied in the inertial subrange is

$$Re_\lambda^{3/4} >>> 1 \tag{13}$$

The representative one-dimensional energy spectra $E_x(k_1)$, $E_y(k_1)$, and $E_z(k_1)$, whose integrals are $\overline{u'^2}$, $\overline{v'^2}$, and $\overline{w'^2}$, are presented in Figures 24*a* and *b*. When $x/D = 40$ and $y/D = 11$ (Figure 24*a*), $k_d \simeq 160$, $k_e < 10^{-1}$, $Re_\lambda \simeq 400$, and $Re_\lambda^4 \simeq 90$. The dissipation rate ϵ was estimated from $\epsilon = 15\nu(\overline{v'^2})/(\lambda_y^2)$ assuming local isotropy. When $x/D = 300$ and $y/D = 30$, $k_d \simeq 80$, $k_e < 10^{-1}$, $Re_\lambda \simeq 300$, and $Re_\lambda^{3/4} \simeq 70$. These values nearly satisfy Equations (11) and (13). One decade of the inertial subrange appears in both Figures 24*a* and *b*. Further, $E_y(k_1)$ is nearly equal to $E_z(k_1)$, and $E_y(k_1)$ and $E_z(k_1)$ are larger than $E_x(k_1)$ in this subrange, which agrees with the locally isotropic inertial subrange relation $E_y(k_1) = E_z(k_1) = 4/3\ E_x(k_1)$. Other spectra obtained for a large number of different locations in the two jets were similar. Hence, we may conclude that the flow field in the interacting two-plane jets is locally isotropic. The spectral equivalent of the hot wire probe element length l_w is also indicated in Figures 24*a* and *b*. For wave numbers less than l_w^{-1}, the effect of wire-length attenuation can be neglected, and the measured spectral values should be good estimates of the true spectra (Champagne et al., 1976).

Probability Density Function

The probability density function $P(u)$ is defined so that $P(u)du$ is the probability that the fluctuating velocity components exists between u and $u + du$. The probability

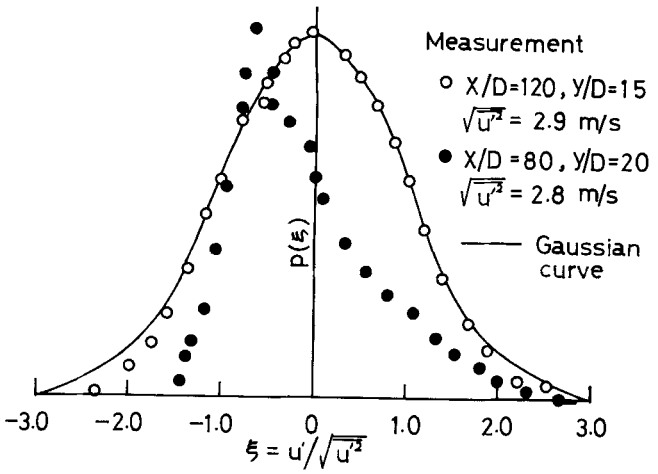

Fig. 25a. Probability density function of the longitudinal fluctuating velocity.

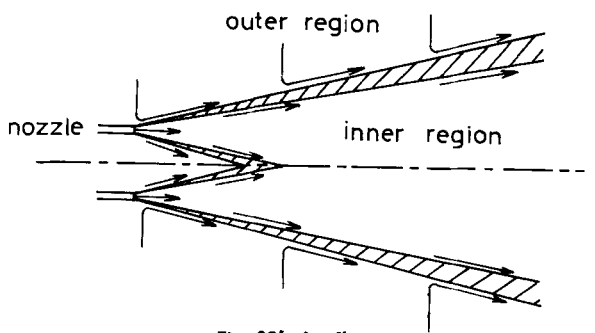

Fig. 25b. Jet flow.

density function of turbulent velocity is often needed for theoretical treatments of turbulence. Hence, it is significant to present the data of probability density function in the interacting two-plane parallel jets. The representative probability density functions are shown in Figure 25*a*. The functions for the most part of the two jets were Gaussian shape which is typical of homogeneous and isotropic turbulence. However, the functions in the shaded portion of Figure 25*b*, where there is a boundary region between inner and outer flow regions of the two jets, departed from Gaussian shape. The departure indicates the presence of strong shear flow. This corresponds to the results in Figure 18.

ACKNOWLEDGMENT

The authors are indebted to T. Tazaki, K. Toya, and T. Nasuno, who performed some of the experimental measurement.

NOTATION

b = jet half width (half distance between the outer points of $U/U_m = 0.5$ as shown in Figure 8)
D = nozzle width
E_x, E_y, E_z = one-dimensional energy spectra whose integrals are u'^2, v'^2, and w'^2, respectively
k_1 = wave number $= 2\pi n/U$
k_d = wave number of main dissipation $= 1/\eta$
k_e = wave number of averaged energy containing eddy
L = distance between the center lines of the two nozzles
l = nozzle length
l_w = hot wire, probe element length
n = frequency
P = probability density function of fluctuating velocity
Re_λ = turbulent Reynolds number $= \sqrt{\overline{v'^2}}\lambda_y/\nu$
$R_{ij_{i=j}}$ = Eulerian autocorrelation coefficient, $R_{11} = R_{xx}$, $R_{22} = R_{yy}$, $R_{33} = R_{zz}$
$R_{ij_{i=j}}$ = Eulerian cross-correlation coefficient, $R_{12} = R_{xy}$
T_{Ei} = Eulerian integral time scale
U = longitudinal time averaged velocity component
U_o = issuing time averaged velocity at jet exit
U_m = maximum time averaged velocity or time averaged jet center-line velocity
$U_{y=0}$ = longitudinal time averaged velocity on the x axis
u', v', w' = longitudinal, lateral and transverse component of fluctuating velocity, respectively
V = lateral time averaged velocity component
x, y, z = coordinates
$\overline{\ }$ = time averaged quantity
$(-)$ = nondimensional coordinates

Greek Letters

ϵ = dissipation rate
η = Kolmogoroff length scale
Λ_x, Λ_y, Λ_z = longitudinal, lateral and transverse Eulerian integral length scales
λ_x, λ_y, λ_z = longitudinal, lateral and transverse Eulerian dissipation scales
ν = kinematic viscosity
τ = delay time
τ_i = Eulerian dissipation time scale

LITERATURE CITED

Baron, T., and E. H. Bollinger, "Mixing of High Velocity Air Jets," *Tech. Rept. No. CML-3*, Engineering Experimental Station, Univ. Ill. (1952).

Becker, H. A., and B. D. Booth, "Mixing in the Interaction Zone of Two Free Jets," *AIChE J.*, **21**, 949-958 (1975).

Bradbury, L. J. S., "The Structure of a Self-Preserving Turbulent Plane Jet," *J. Fluid Mech.*, **23**, 31-64 (1965).

Champagne, F. H., Y. H. Pao, and I. J. Wygnanski, "On the Two-Dimensional Mixing Region," *ibid.*, 74, 209-250 (1976).

Corrsin, S., "Investigation of the Behavior of Parallel Two-Dimensional Air Jets," *NACA ACR*, No. 4H24 (1944).

Gutmark, E., and I. J. Wygnanski, "The Planar Turbulent Jet," *J. Fluid Mech.*, **73**, 465-495 (1976).

Kirillov, V. A., and B. G. Khudenko, "Calculation of the Direction of the Axis of a Stream Resulting from the Mixing of Turbulent Jets," *J. Eng. Phys.*, **9**, 414-415 (1965).

Knystautas, R., "The Turbulent Jet from a Series of Holes in Line," *Aeronautical Quarterly*, **15**, 1-28 (1964).

Makarov, I. S., and B. G. Khudenko, "Mixing of Intersecting Turbulent Jets," *J. Eng. Phys.*, **8**, 304-306 (1965).

Marsters, G. F., "Interaction of Two Plane, Parallel Jets," *AIAA J.*, **15**, 1756-1762 (1977).

Miller, D. R., and E. W. Comings, "Force-momentum Field in a Dual-Jet Flow," *J. Fluid Mech.*, **7**, 237-256 (1960).

Rummel, K., *Der einfluss des Mischvorganges auf die Verbrennung von Gas unt Luft in Feuerungen*, Verlag Stahleisen, Dusseldorf, Germany (1937).

Tanaka, E., "The Interference of Two-Dimensional Parallel jets (1st Report, Experiments on Dual Jet)," *Bull. JSME*, **13**, 272-280 (1970).

———, "The Interference of Two-Dimensional Parallel Jets (2nd Report Experiments on the Combined Flow of Dual Jet)," *ibid.*, **17**, 920-970 (1974).

Trantacoste, N., and P. Sforza, "Further Experimental Results for Three-Dimensional Free Jets," *AIAA J.*, **5**, 885-891 (1967).

Manuscript received August 4, 1978; revision received February 9, and accepted February 20, 1979.